PHYSICAL REVIEW LETTERS **121,** 075101 (2018)

Featured in Physics

Two-Dimensional Solar Wind Speeds from 6 to 26 Solar Radii in Solar Cycle 24 by Using Fourier Filtering

Il-Hyun Cho,[1] Yong-Jae Moon,[1,*] Valery M. Nakariakov,[1,2] Su-Chan Bong,[3,4] Jin-Yi Lee,[1]
Donguk Song,[5] Harim Lee,[1] and Kyung-Suk Cho[3,4]
[1]*Kyung Hee University, Yongin-si, Gyeonggi-do, 17104, Korea*
[2]*University of Warwick, Coventry CV4 7AL, United Kingdom*
[3]*Korea Astronomy and Space Science Institute, Yuseong-gu, Daejeon 34055, Korea*
[4]*University of Science and Technology, Yuseong-gu, Daejeon 34113, Korea*
[5]*National Institutes of Natural Sciences, Mitaka, Tokyo 181-8588, Japan*

(Received 12 January 2018; revised manuscript received 28 May 2018; published 14 August 2018)

Measurement of the solar wind speed near the Sun is important for understanding the acceleration mechanism of the solar wind. In this Letter, we determine 2D solar wind speeds from 6 to 26 solar radii by applying Fourier motion filters to *SOHO*/LASCO C3 movies observed from 1999 to 2010. Our method successfully reproduces the original flow speeds in the artificially generated data as well as streamer blobs. We measure 2D solar wind speeds from one-day to one-year timescales and their variation in solar cycle 24. We find that the solar wind speeds at timescales longer than a month in the solar maximum period are relatively uniform in the azimuthal direction, while they are clearly bimodal in the minimum period, as expected from the Ulysses observations and interplanetary radio scintillation reconstruction. The bimodal structure appears at around 2006, becomes most distinctive in 2009, and abruptly disappears in 2010. The radial evolution of the solar wind speeds resembles the Parker's solar wind solution.

DOI: 10.1103/PhysRevLett.121.075101

Introduction.—The solar wind is a magnetized plasma emanated from the Sun [1,2], which disturbs the planet's atmosphere [3] and forms the heliosphere [4]. Early *in situ* observations of the solar wind were performed mainly in the equatorial plane. *Mariner 2* observed the continuous and fast solar wind in the range 0.7–1 AU [5], first confirming that the solar wind is the result of expansion of the hot solar corona [6]. *Helios* spacecrafts observed important kinetic properties of solar wind in the range 0.3–1 AU (e.g., [7]). The *Pioneer* mission explored the outer heliosphere and found a large scale radial structure of solar wind [8]. The *Ulysses* spacecraft first explored the plasma property of the heliosphere in high latitude over ±80° [9], providing the direct measurement of the latitudinal structure of the solar wind [10]. *In situ* observations have been performed continuously by a series of near Earth satellites such as the *Interplanetary Monitoring Platform*, *Advanced Composition Explorer*, and *Wind*.

Early spectroscopic measurements in the ultraviolet acquired with rockets and space shuttles provided plasma properties in detail for the extended corona below 5 solar radii [11], revealing that the sonic height of the solar winds is ∼2 solar radii [12–14]. It is also found that the line-of-sight (LOS) velocity has multiple components [15]. Since then, systematic observations by the Ultraviolet Coronagraph Spectrometer [16] on board the *Solar and Heliospheric Observatory* (*SOHO*) [17] have enabled us to study the plasma property in the extended corona in several aspects: large scale characteristics [18,19], its evolution in the solar cycle [20,21], streamers [22], coronal plumes [23], and coronal mass ejections (CMEs) [24]. In particular, outflow speeds of protons and heavy ions were calculated by using a Doppler dimming technique [25,26] for various latitudes and phases of solar cycle [20,27–38], revealing how the solar wind speed evolves in the extended corona.

The radio scintillation in the interplanetary space enables exploration of the spatial structure of solar wind speed in the inner part of the interplanetary space from ground-based observatories in timescales typically longer than a few days. It is found that the acceleration of solar wind speed in the South Pole measured by the interplanetary radio scintillation (IPS) technique is almost complete at 10 solar radii, suggesting that the acceleration is strongly linked to the coronal heating [39]. The solar wind speed from 1.5 to 20.5 solar radii for a wide latitudinal range measured by applying the IPS observation on the radio signals from the *Venus Explorer* suggests that the supply of plasma from closed loops to the solar wind occurs over an extended area [40]. The observations with many astrophysical objects combined with a tomographic reconstruction provides the global structure of solar wind [41,42].

As the continuous and homogeneous coronagraphic measurements of scattered light by coronal plasma become possible, the radial evolution of the solar wind speed could be traced in timescales shorter than those of the IPS observations. The radial speeds tracked by the heights of streamer blobs observed by the Large Angle and Spectroscopic Coronagraph (LASCO) [43] on-board the *SOHO* are well characterized by the Parker's solar wind that isothermally expanded at a temperature of 1.1 MK and a sonic point near 5 solar radii, interpreting that the speeds are a passive tracer of the solar wind [44]. The radial speeds tracked by slowly evolving CMEs from 2 to 30 solar radii are well fit to a power law with the exponent lower than 1.0 [45], which is similar to the profile of streamer blobs [44]. Recently, these structures are traced up to ~50° from the Sun [46,47], which provide detailed information on the dynamical evolution of the structures in the interplanetary space far from the Sun.

A few attempts to examine the 2D structure of solar wind speed have been made in order to understand its dynamical properties in the low corona. For example, polar solar wind speeds in the low corona ranging from 2.8 to 10 solar radii, which are calculated where the cross-correlation is high (e.g., [48,49]), were found to be a mixture of intermittent slow and fast patches of material [50]. Decelerations of the solar wind at ~1.5 solar radii at the poles and ~2 solar radii at the equator were detected by analyzing the Doppler dimming [25,26] from the reconstructed images of the polarized brightness and ultraviolet [38]. Here, we determine 2D solar wind speeds from 6 to 26 solar radii using coronagraphic observations.

Data and Method.—Since 1996, the *SOHO*/LASCO C3 instrument provides continuous and homogeneous data sets of white-light coronagraphic observations near the Sun (4–30 solar radii) where most of the dynamical evolution of eruptions and the wind acceleration would be completed. The coronagraphic white-light image largely shows CMEs [47,51,52] associated plasma outflows [53–56], shocks [57,58], streamer blobs [59], and jets [60] that are very dynamic. It also contains less dynamic features such as streamers [22], but these structures are likely to fade in the outer corona and be observed as flowing structures [61]. All these dynamic and faint features can be decomposed into a series of movies as a function of speed by applying the Fourier motion filters [62] which have been successfully applied to detect the faint inbound motion reflected due to an Alfvén surface (e.g., [63]) in the corona, by keeping the first and third quadrants of the Fourier spectrum of a height-time image.

We use open-access LASCO C3 images from 1999 to 2010 of which the number of images for three consecutive days exceeds 108. An imaging data cube is obtained by sequentially taking the level 0.5 images that have been rectified to put the solar north at the top of the image, by using the SOLARSOFT [64] function mk_img.pro with the keywords rectified and log_scl. After removing few bad images, we obtain one movie $I(x,y,t)$ for three days which has a size of $1024 \times 1024 \times n$, where n is the number of images during three days which typically exceeds 100.

We use a normalized movie $N(x,y,t)$ by taking $(I - I_{\mathrm{MED}})/I_{\mathrm{MAD}}$ for a given pixel, where I_{MED} and I_{MAD} represent the median and median absolute deviation of $I(t)$. We further suppress the intensity of stars and planets into $0 \pm 5\sigma$. Their speeds in the movie are similar to the speed of the Earth's revolution ($\sim 30\ \mathrm{km\,s^{-1}}$) so that its contribution to solar wind speeds is minor. We transform the movie into the polar coordinate (r,θ,t) centered on the Sun, with the size of $505 \times 1444 \times n$. The transformed image for a given time is spatially remapped to 128×360 size to increase the signal to noise ratio. Then, the movie is temporally interpolated with a cadence of 33.75 min (equal to 72 hours/128), giving a movie $I(\theta,r,t)$ with the size of $128 \times 360 \times 128$. Thus, for a given azimuthal angle, the size of the height-time image is 128×128.

The movie is decomposed into a series of movies as a function of speed by performing the inverse Fourier transform for the filtered spectrum of the height-time image, with varying pass bands of phase speed for a given azimuthal angle as follows:

$$N(r,\theta_i,t,v_j) = \mathcal{F}^{-1}_{r,t}\{\mathcal{F}_{r,t}\{I(r,\theta_i,t)\}G(k,w)_{v_j}\}, \quad (1)$$

where θ_i ranges 0–360° with the sampling size of 1°. The phase speed filters that pass the powers around v_j (0, 30, 60, …, 2010 $\mathrm{km\,s^{-1}}$) are defined as follows:

$$G(k,w)_{v_j} = e^{-(v-v_j)^2/2\sigma_v^2} \times \{e^{-(k-k_m)^2/2\sigma_k^2} + e^{-(k+k_m)^2/2\sigma_k^2}\} \times \{e^{-(\omega-\omega_m)^2/2\sigma_w^2} + e^{-(\omega+\omega_m)^2/2\sigma_w^2}\}, \quad (2)$$

where v, σ_v, k_m, σ_k, ω_m, σ_ω are w/k, $30\ \mathrm{km\,s^{-1}}$, $(5r_{Sun})^{-1}$, $(6r_{Sun})^{-1}$, $(5\ \mathrm{hours})^{-1}$, $(6\ \mathrm{hours})^{-1}$, respectively. The operators $\mathcal{F}\{\}$ and $\mathcal{F}^{-1}\{\}$ are the Fourier transform and inverse Fourier transform, respectively. The latter two terms are low pass filters in the wave number and frequency domain, which are symmetric with respect to zero wave number or frequency so that the powers around zero slightly decrease when compared to those at the mean values. This may suppress the effect of large scale gradients possibly remaining in the movie. Then, we define $N^2(r,\theta,t,v)$ as the speed histogram $P(r,\theta,t,v)$. Thus, the solar wind speed and its standard deviation are defined as follows:

$$V(r,\theta,t) = \sum_v vP(r,\theta,t)/\sum_v P(r,\theta,t),$$

$$\sigma_V(r,\theta,t) = \sqrt{\sum_v (v-V)^2 P(r,\theta,t)/\sum_v P(r,\theta,t)}. \quad (3)$$

We note that original $\sigma_V(r,\theta,t)$ ranges 100–700 $\mathrm{km\,s^{-1}}$ which is rather large compared to $V(r,\theta,t)$, implying that a speed histogram likely has multiple peaks or a broad distribution. It is possibly due to multiple velocity components or low signal-to-noise ratio. In addition, three projection effects can partly contribute to the errors.

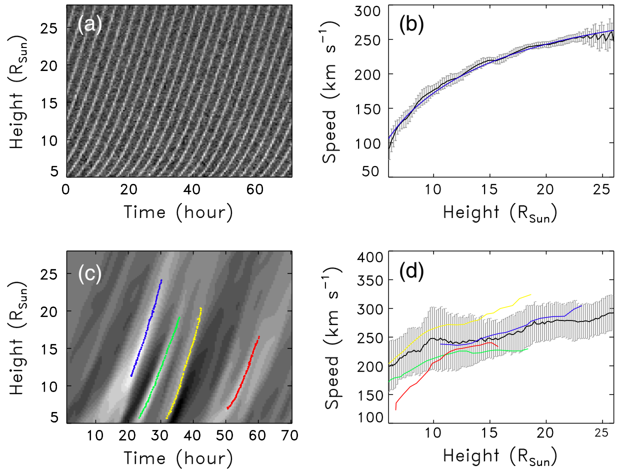

FIG. 1. Height-time images of artificially generated moving intensity features [white in panel (a)], streamer blobs observed by LASCO C3 from September 26, 2007 to September 28, 2007 at an azimuthal angle equal to 334° [white in panel (c)], and comparisons of the estimated speeds by applying a Fourier motion filter with true speeds [(b) and (d)]. In the right panels, the estimated speeds are indicated by black solid lines. The true speeds are indicated by blue, green, yellow, and red lines. The grey vertical bars indicated in the right panels are the median absolute deviations during three days at each height.

First, our measurements are based on 2D observations that integrate scattered photons on a LOS, which includes different heights from the Sun for a given position. Second, there is an offset between the solar equator and the observed center of the Sun, which ranges approximately ±7°. Third, an original movie covers three days which ranges 40–43° of longitude depending on latitude. Thus, we take the central day from the movie to obtain the map of a one day median, which includes ~42 samples. If we assume the error is inversely proportional to the square root of the number of samples when averaging, the median absolute deviation (0.6745σ) becomes 10–72 km s^{-1}, which may be acceptable for an application level.

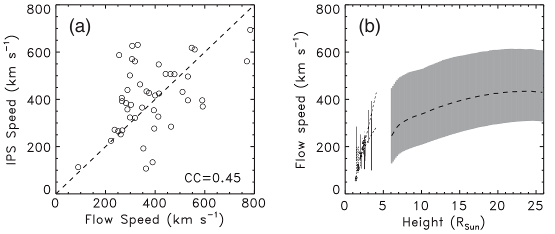

FIG. 2. Comparisons of the solar wind speeds obtained from LASCO C3 with IPS speeds (a) and radial speeds of protons given by a Doppler dimming technique below "six" solar radii (b). In panel (a), the IPS speeds are interpolated from the projected speeds [65] based on the position and time of our data sets covering whole latitudes. In panel (b), the radial speeds of protons are measured in the extended corona above coronal holes that have been taken from [38], and the estimated electron speed in 6–26 solar radii is taken from the North and South Poles. The grey area indicates 1-σ interval.

As shown in Fig. 1, the estimated speeds by using the Fourier filtering are well consistent with the true speeds, indicating that the method properly detects solar wind speeds from pseudoreal and real height-time images. In Fig. 1(b), the true speed (blue) is defined as $300\sqrt{e^{-(r-4)/15}}$ km s^{-1} to simulate the height-time map [Fig. 1(a)] that is constructed by stacking time-shifted-intensity pulses along the heights.

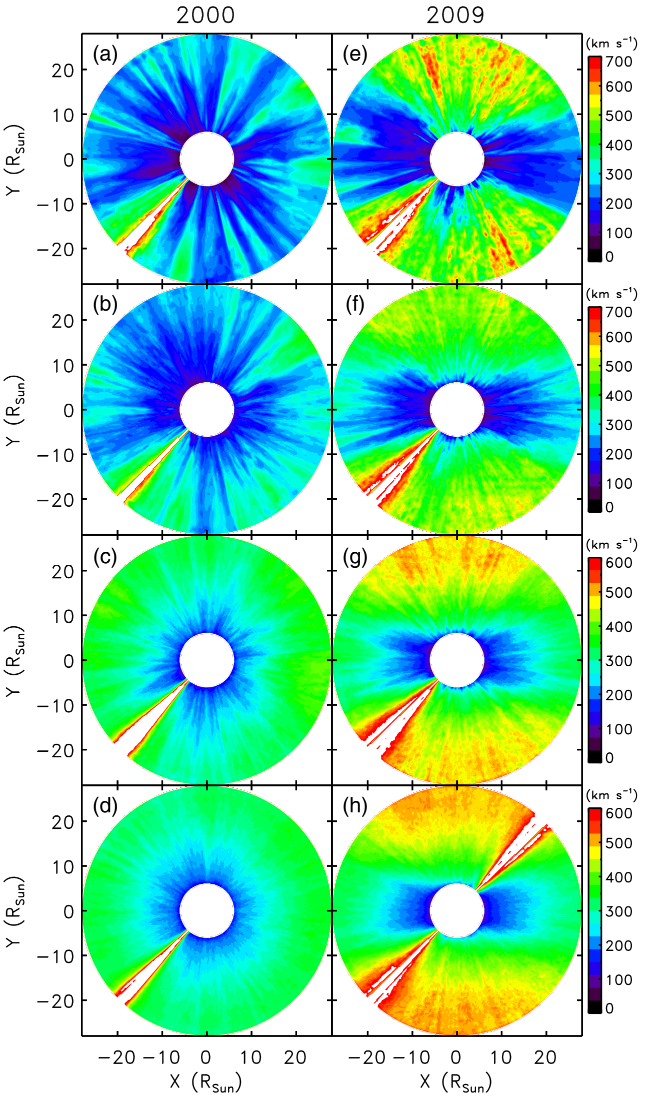

FIG. 3. Maps of median solar wind speeds in 6–26 solar radii over several time periods (one day to one year) in 2000 (a)–(d) and 2009 (e)–(h). The one-day maps are constructed by taking the median solar wind speed at each position during 00–24 UT on October 4, 2000 (a) and March 7, 2009 (e). The one-week maps are constructed by taking the median solar wind speed at each position during October 4, 2000 12 UT ± 3.5 days (b) and March 7, 2009 12 UT ± 3.5 days (f). The one-month maps are constructed from maps of daily solar wind speed in July 2000 (c) and February 2009 (g). The one-year maps are constructed from maps of monthly solar wind speed in 2000 (d) and 2009 (h).

In Fig. 1(d), the true speeds (colored lines) are instantaneous speeds calculated from manually determined height-time data in Fig. 1(c). The height-time image of streamer blobs [Fig. 1(c)] is filtered by a broadband Gaussian filter ($200 \pm 100\ \mathrm{km\ s^{-1}}$) to improve the visibility of the signal.

It seems that our measurements are roughly consistent with previous ones. In Fig. 2(a), we compare $V(r, \theta, t)$ with IPS solar wind speeds [65] which are projected to the sky plane during 1999–2010. The IPS observations are mostly contributed by the plasma located at the closest position in the LOS between the observer and a radio source, see, e.g., [42,66]. Here, we chose the IPS samples with a velocity error less than 10 $\mathrm{km\,s^{-1}}$ and interpolated the position and time to those of our data sets. The correlation coefficient (CC) is 0.45 and its significance level is less than 0.01. The marginal CC may be due to the difference of characteristic sizes of the local plasma detected by IPS and the white-light coronagraph. In Fig. 2(b), we plot the $V(r, \theta, t)$ obtained at 90° and 270° from 1999 to 2010 onto the collection of proton outflow speeds in coronal holes derived from a Doppler dimming technique (see [38]), which may be well connected to the electron speed within 1-σ intervals (grey area).

Results.—By using this method, we obtain the maps of the solar wind speed with timescales of half an hour from 1999 to 2010. From this, we determined the maps of the solar wind speed from one day to one year. The spatial structure of the solar wind speed is generally believed to be homogeneous with respect to the solar latitude in the solar maximum period because of the frequent appearance of nonpolar coronal holes and CMEs in the solar corona. On the other hand, it shows a bimodal structure in the solar minimum period: mainly fast winds are detected in the polar regions and slow winds in the equatorial regions [67]. Figure 3 shows maps of median solar wind speeds over several time periods of sampling (one day to one year) in 2000 and 2009. It is shown that the intrinsic features of the latitudinal distribution of the solar wind speed seem to become evident as the sampling time period becomes longer. In 2000, the median solar wind maps over short time periods in Figs. 3(a) and 3(b) show fast speeds with approximately 400 $\mathrm{km\,s^{-1}}$ for a specific latitude, possibly contributed by moving features such as CMEs and streamer blobs. However, the uniform distribution of the solar wind speed with latitude appears in the monthly median. In 2009, the bimodal structure of solar wind speed becomes apparent in the one-week median map as in Fig. 3(f). Thus, we confirm the uniformity and bimodality of the spatial structure of the solar wind speeds in the inner part of the interplanetary space, which are consistent with previous observations of the outer heliosphere [68,69] as well as of the extended corona below 6 solar radii (e.g., [38,70]). More precise quantitative measurement can be obtained by future space observations such as the *Parker Solar Probe* [71,72], METIS coronagraph [73,74] on-board Solar Orbiter [75], and *ISS* Coronagraph [76,77].

The uniform and bimodal structures are more clear in the yearly maps of the solar wind speed as seen in Fig. 4. The uniform latitudinal distribution is observed at the starting year and maintained during the solar maximum period (1999–2004). The latitudinal structure of the solar wind speed does not seem to change dramatically during the maximum period. It is evident that the bimodal structure started to appear in 2005 and grew until 2009 which corresponds to the solar minimum. The structure in 2009 is the most apparent. The polar solar wind speed seems to increase as the solar activity goes to the activity minimum which is similar to the result given by [78]. The bimodal structure disappears and becomes uniform around 2010 which corresponds to the beginning of the new solar cycle 24.

In Fig. 5, radial profiles of solar wind speeds near the solar poles and equator in the one-year map in 2000 and 2009 are presented. The profiles are well matched with the

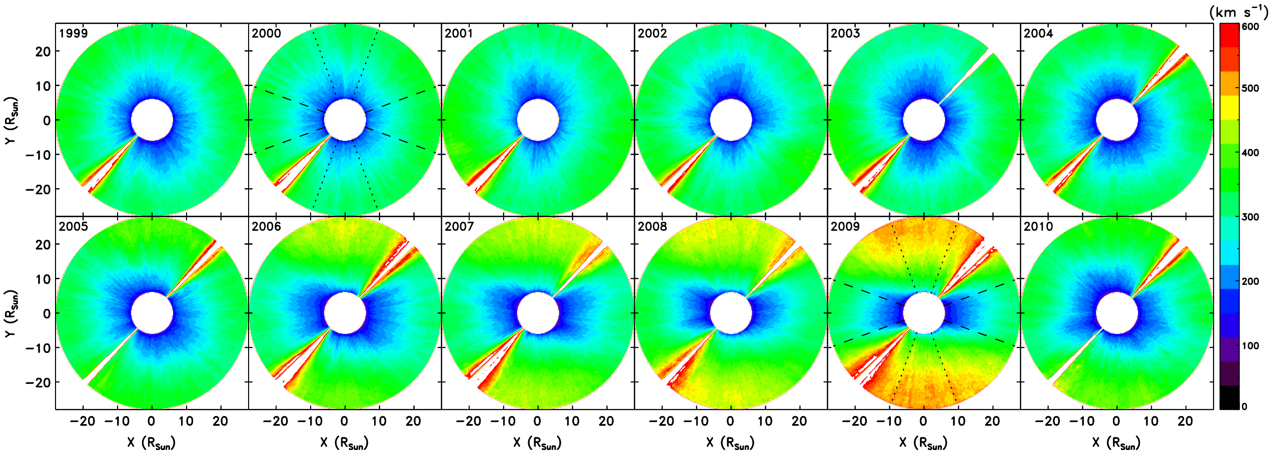

FIG. 4. Maps of yearly median solar wind speeds from 1999 to 2010. The two dotted lines in 2000 and 2009 indicate ±20° from the North and South Poles. The two dashed lines in 2000 and 2009 indicate ±20° from the equator.

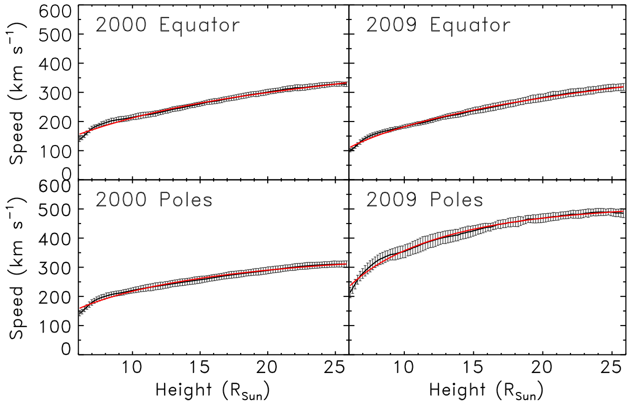

FIG. 5. Radial profiles of equatorial and polar solar wind speeds in the one-year maps of 2000 and 2009. The black lines represent the observed speeds averaged over ±20° from the equator and poles indicated by dashed and dotted lines in Fig. 4, respectively. The vertical bars are the corresponding standard deviations. The red lines represent the model speeds obtained from the least squares fit by the function defined as $v_0\sqrt{1-e^{-(r-r_1)/r_0}}$.

function $v_0\sqrt{1-e^{-(r-r_1)/r_0}}$, which describes a rapid acceleration until $r \sim r_1$ and approaches the asymptotic speed v_0 at $r - r_1 \gg r_0$ [44], resembling the Parker's solar wind solution. In other words, the acceleration is rapid in the initial stage and exponentially decreases with height. Our result is consistent with the previous indirect observation that the polar solar wind is mainly accelerated below 10 solar radii and then continues at a nearly constant speed [39].

The 2D solar wind speeds in various timescales from one day to 11 years determined in this Letter could be compared with measurements in the heliosphere [2,79,80], and possibly in astrospheres [81]. The propagation of CMEs is affected by the properties of CME itself as well as the background wind speed (e.g., [82–88]). Thus, we hope that our results would be used to improve the accuracies of CME arrival times (e.g., [89,90]). The speeds also provide constraints on the solar wind models (e.g., [91–95]), which would improve our understanding of the dynamical properties of the solar wind.

We appreciate the constructive comments from an anonymous referee which improved the manuscript. The *SOHO*/LASCO data used here are produced by a consortium of the Naval Research Laboratory (USA), Max-Planck-Institut for Sonnensystemforschung (Germany), Laboratoire d'Astrophysique Marseille (France), and the University of Birmingham (United Kingdom). *SOHO* is a project of international cooperation between ESA and NASA. This research is supported by the Korea Astronomy and Space Science Institute under the R&D program, Development of a Solar Coronagraph on the International Space Station (Project No. 2017-1-851-00), supervised by the Ministry of Science and ICT. It is also supported by the Brain Korea 21 plus program through the National Research Foundation (NRF) funded by the Ministry of Education of Korea. Y. J. M. acknowledges support from the Basic Science Research Program through the NRF funded by the Ministry of Korea (Grant No. NRF-2016R1A2B4013131) and NRF of Korea Grant funded by the Korean Government (Grant No. NRF-2013M1A3A3A02042232). V. M. N. is supported by the STFC consolidated Grant No. ST/P000320/1. J. Y. L. is supported by Basic Science Research Program though the NRF funded by the Ministry of Education of Korea (Grant No. NRF-2016R1A6A3A11932534).

---

[*] moonyj@khu.ac.kr

[1] T. Sakao, R. Kano, N. Narukage, J. Kotoku, T. Bando, E. E. DeLuca, L. L. Lundquist, S. Tsuneta, L. K. Harra, Y. Katsukawa *et al.*, Science **318**, 1585 (2007).
[2] L. Abbo, L. Ofman, S. K. Antiochos, V. H. Hansteen, L. Harra, Y.-K. Ko, G. Lapenta, B. Li, P. Riley, L. Strachan *et al.*, Space Sci. Rev. **201**, 55 (2016).
[3] R. Lundin, S. Barabash, H. Andersson, M. Holmström, A. Grigoriev, M. Yamauchi, J.-A. Sauvaud, A. Fedorov, E. Budnik, J.-J. Thocaven *et al.*, Science **305**, 1933 (2004).
[4] K. Dialynas, S. M. Krimigis, D. G. Mitchell, R. B. Decker, and E. C. Roelof, Nat. Astron. **1**, 0115 (2017).
[5] M. Neugebauer and C. W. Snyder, J. Geophys. Res. **71**, 4469 (1966).
[6] E. N. Parker, Astrophys. J. **128**, 664 (1958).
[7] E. Marsch, H. Rosenbauer, R. Schwenn, and K.-H. Muehlhaeuser, J. Geophys. Res. **87**, 35 (1982).
[8] S. E. Kayser, A. Barnes, and J. D. Mihalov, Astrophys. J. **285**, 339 (1984).
[9] J. A. Simpson, M. Zhang, and S. Bame, Astrophys. J. Lett. **465**, L69 (1996).
[10] E. J. Smith, R. G. Marsden, and D. E. Page, Science **268**, 1005 (1995).
[11] S. R. Cranmer, J. L. Kohl, G. Noci, E. Antonucci, G. Tondello, M. C. E. Huber, L. Strachan, A. V. Panasyuk, L. D. Gardner, M. Romoli *et al.*, Astrophys. J. **511**, 481 (1999).
[12] G. L. Withbroe, J. L. Kohl, H. Weiser, G. Noci, and R. H. Munro, Astrophys. J. **254**, 361 (1982).
[13] J. L. Kohl, H. Weiser, G. L. Withbroe, C. A. Zapata, and R. H. Munro, Bull. Am. Astron. Soc. **16**, 531 (1984).
[14] L. Strachan, J. L. Kohl, H. Weiser, G. L. Withbroe, and R. H. Munro, Astrophys. J. **412**, 410 (1993).
[15] J. L. Kohl, L. D. Gardner, L. Strachan, R. Fisher, and M. Guhathakurta, Space Sci. Rev. **72**, 29 (1995).
[16] J. L. Kohl, R. Esser, L. D. Gardner, S. Habbal, P. S. Daigneau, E. F. Dennis, G. U. Nystrom, A. Panasyuk, J. C. Raymond, P. L. Smith *et al.*, Sol. Phys. **162**, 313 (1995).
[17] V. Domingo, B. Fleck, and A. I. Poland, Sol. Phys. **162**, 1 (1995).
[18] L. Zangrilli, P. Nicolosi, G. Poletto, G. Noci, M. Romoli, and J. L. Kohl, Astron. Astrophys. **342**, 592 (1999). http://aa.springer.de/papers/9342002/2300592.pdf.
[19] L. Strachan, A. V. Panasyuk, D. Dobrzycka, J. L. Kohl, G. Noci, S. E. Gibson, and D. A. Biesecker, J. Geophys. Res. **105**, 2345 (2000).

[20] M. P. Miralles, S. R. Cranmer, and J. L. Kohl, Astrophys. J. Lett. **560**, L193 (2001).

[21] R. Ventura, D. Spadaro, G. Cimino, and M. Romoli, Astron. Astrophys. **430**, 701 (2005).

[22] L. Abbo, R. Lionello, P. Riley, and Y.-M. Wang, Sol. Phys. **290**, 2043 (2015).

[23] N.-E. Raouafi, J. W. Harvey, and S. K. Solanki, Astrophys. J. **658**, 643 (2007).

[24] J.-Y. Lee, J. C. Raymond, Y.-K. Ko, and K.-S. Kim, Astrophys. J. **692**, 1271 (2009).

[25] G. L. Withbroe, J. L. Kohl, H. Weiser, and R. H. Munro, Space Sci. Rev. **33**, 17 (1982).

[26] G. Noci, J. L. Kohl, and G. L. Withbroe, Astrophys. J. **315**, 706 (1987).

[27] L. Strachan, Y.-K. Ko, A. V. Panasyuk, D. Dobrzycka, J. L. Kohl, M. Romoli, G. Noci, S. E. Gibson, and D. A. Biesecker, Space Sci. Rev. **87**, 311 (1999).

[28] E. Antonucci, M. A. Dodero, and S. Giordano, Sol. Phys. **197**, 115 (2000).

[29] M. P. Miralles, S. R. Cranmer, A. V. Panasyuk, M. Romoli, and J. L. Kohl, Astrophys. J. Lett. **549**, L257 (2001).

[30] L. Zangrilli, G. Poletto, P. Nicolosi, G. Noci, and M. Romoli, Astrophys. J. **574**, 477 (2002).

[31] R. A. Frazin, S. R. Cranmer, and J. L. Kohl, Astrophys. J. **597**, 1145 (2003).

[32] L. Teriaca, G. Poletto, M. Romoli, and D. A. Biesecker, Astrophys. J. **588**, 566 (2003).

[33] A. H. Gabriel, L. Abbo, F. Bely-Dubau, A. Llebaria, and E. Antonucci, Astrophys. J. Lett. **635**, L185 (2005).

[34] D. Telloni, E. Antonucci, and M. A. Dodero, Astron. Astrophys. **472**, 299 (2007).

[35] L. Zangrilli and G. Poletto, Astron. Astrophys. **545**, A8 (2012).

[36] S. Dolei, D. Spadaro, and R. Ventura, Astron. Astrophys. **577**, A34 (2015).

[37] S. Dolei, D. Spadaro, and R. Ventura, Astron. Astrophys. **592**, A137 (2016).

[38] A. Bemporad, Astrophys. J. **846**, 86 (2017).

[39] R. R. Grail, W. A. Coles, M. T. Klinglesmith, A. R. Breen, P. J. S. Williams, J. Markkanen, and R. Esser, Nature (London) **379**, 429 (1996).

[40] T. Imamura, M. Tokumaru, H. Isobe, D. Shiota, H. Ando, M. Miyamoto, T. Toda, B. Häusler, M. Pätzold, A. Nabatov *et al.*, Astrophys. J. **788**, 117 (2014).

[41] M. Kojima, M. Tokumaru, H. Watanabe, A. Yokobe, K. Asai, B. V. Jackson, and P. L. Hick, J. Geophys. Res. **103**, 1981 (1998).

[42] P. K. Manoharan, Astrophys. J. **751**, 128 (2012).

[43] G. E. Brueckner, R. A. Howard, M. J. Koomen, C. M. Korendyke, D. J. Michels, J. D. Moses, D. G. Socker, K. P. Dere, P. L. Lamy, A. Llebaria *et al.*, Sol. Phys. **162**, 357 (1995).

[44] N. R. Sheeley, Y.-M. Wang, S. H. Hawley, G. E. Brueckner, K. P. Dere, R. A. Howard, M. J. Koomen, C. M. Korendyke, D. J. Michels, S. E. Paswaters *et al.*, Astrophys. J. **484**, 472 (1997).

[45] A. Shanmugaraju, Y.-J. Moon, B. Vrsnak, and D. Vrbanec, Sol. Phys. **257**, 351 (2009).

[46] N. R. Sheeley, Jr., D. D.-H. Lee, K. P. Casto, Y.-M. Wang, and N. B. Rich, Astrophys. J. **694**, 1471 (2009).

[47] A. P. Rouillard, N. R. Sheeley, Jr., T. J. Cooper, J. A. Davies, B. Lavraud, E. K. J. Kilpua, R. M. Skoug, J. T. Steinberg, A. Szabo, A. Opitz, and J.-A. Sauvaud, Astrophys. J. **734**, 7 (2011).

[48] S. J. Tappin, G. M. Simnett, and M. A. Lyons, Astron. Astrophys. **350**, 302 (1999). http://aa.springer.de/papers/9350001/2300302.pdf.

[49] D. J. Lewis and G. M. Simnett, Mon. Not. R. Astron. Soc. **333**, 969 (2002).

[50] B. V. Jackson, H.-S. Yu, A. Buffington and P. P. Hick, Astrophys. J. **793**, 54 (2014).

[51] X. Cheng, M. D. Ding, Y. Guo, J. Zhang, A. Vourlidas, Y. D. Liu, O. Olmedo, J. Q. Sun, and C. Li, Astrophys. J. **780**, 28 (2014).

[52] H. Hu, Y. D. Liu, R. Wang, X. Zhao, B. Zhu, and Z. Yang, Astrophys. J. **840**, 76 (2017).

[53] Y.-K. Ko, J. C. Raymond, J. Lin, G. Lawrence, J. Li, and A. Fludra, Astrophys. J. **594**, 1068 (2003).

[54] P. Kumar and K.-S. Cho, Astron. Astrophys. **557**, A115 (2013).

[55] D. F. Webb and A. Vourlidas, Sol. Phys. **291**, 3725 (2016).

[56] J. Chae, K. Cho, R.-Y. Kwon, and E.-K. Lim, Astrophys. J. **841**, 49 (2017).

[57] J.-O. Lee, Y.-J. Moon, J.-Y. Lee, K.-S. Lee, S. Kim, and K. Lee, Astrophys. J. Lett. **796**, L16 (2014).

[58] R.-Y. Kwon and A. Vourlidas, Astrophys. J. **836**, 246 (2017).

[59] H. Q. Song, Y. Chen, K. Liu, S. W. Feng, and L. D. Xia, Sol. Phys. **258**, 129 (2009).

[60] R. L. Moore, A. C. Sterling, and D. A. Falconer, Astrophys. J. **806**, 11 (2015).

[61] C. E. DeForest, W. H. Matthaeus, N. M. Viall, and S. R. Cranmer, Astrophys. J. **828**, 66 (2016).

[62] C. E. DeForest, T. A. Howard, and D. J. McComas, Astrophys. J. **787**, 124 (2014).

[63] A. Verdini, M. Velli, and E. Buchlin, Astrophys. J. Lett. **700**, L39 (2009).

[64] http://www.mssl.ucl.ac.uk/surf/sswdoc/solarsoft.

[65] ftp://ftp.isee.nagoya-u.ac.jp/pub/vlist/.

[66] J. M. Sokół, M. Bzowski, M. Tokumaru, K. Fujiki, and D. J. McComas, Sol. Phys. **285**, 167 (2013).

[67] J. L. Phillips, S. J. Bame, A. Barnes, B. L. Barraclough, W. C. Feldman, B. E. Goldstein, J. T. Gosling, G. W. Hoogeveen, D. J. McComas, M. Neugebauer, and S. T. Suess, Geophys. Rev. Lett. **22**, 3301 (1995).

[68] M. Kojima and T. Kakinuma, Space Sci. Rev. **53**, 173 (1990).

[69] D. J. McComas, B. L. Barraclough, H. O. Funsten, J. T. Gosling, E. Santiago-Muñoz, R. M. Skoug, B. E. Goldstein, M. Neugebauer, P. Riley, and A. Balogh, J. Geophys. Res. **105**, 10419 (2000).

[70] S. Dolei, R. Susino, C. Sasso, A. Bemporad, V. Andretta, D. Spadaro, R. Ventura, E. Antonucci, L. Abbo, V. Da Deppo *et al.*, Astron. Astrophys. **612**, A84 (2018).

[71] https://www.nasa.gov/content/goddard/parker-solar-probe.

[72] N. J. Fox, M. C. Velli, S. D. Bale, R. Decker, A. Driesman, R. A. Howard, J. C. Kasper, J. Kinnison, M. Kusterer, D. Lario *et al.*, Space Sci. Rev. **204**, 7 (2016).

[73] S. Fineschi, E. Antonucci, G. Naletto, M. Romoli, D. Spadaro, G. Nicolini, L. Abbo, V. Andretta, A. Bemporad,

A. Berlicki *et al.*, Proc. SPIE Int. Soc. Opt. Eng. **8443**, 84433H (2012).

[74] E. Antonucci, V. Andretta, S. Cesare, A. Ciaravella, G. Doschek, S. Fineschi, S. Giordano, P. Lamy, D. Moses, G. Naletto *et al.*, Proc. SPIE Int. Soc. Opt. Eng. **10566**, 105660L (2017).

[75] D. Müller and O. C. St. Cyr, Proc. SPIE Int. Soc. Opt. Eng. **8862**, 88620E (2013).

[76] K.-S. Cho, S.-C. Bong, S. Choi, H. Yang, J. Kim, J.-H. Baek, J. Park, E.-K. Lim, R.-S. Kim, S. Kim *et al.*, J. Korean Astron. Soc. **50**, 139 (2017).

[77] H. Yang, S.-C. Bong, K.-S. Cho, S. Choi, J. Park, J. Kim, J.-H. Baek, J. Nah, M. Sun, and Q. Gong, J. Korean Astron. Soc. **51**, 27 (2018).

[78] M. Tokumaru, M. Kojima, and K. Fujiki, J. Geophys. Res. **115**, A04102 (2010).

[79] M. M. Bisi, R. A. Fallows, B. V. Jackson, M. Tokumaru, A. Gonzalez-Esparza, J. Morgan, I. V. Chashei, J. Mejia-Ambriz, S. A. Tyul'bashev, P. K. Manoharan *et al.*, American Geophysical Union, Report No. SH21A-2648, 2017 (unpublished).

[80] https://omniweb.gsfc.nasa.gov/.

[81] B. E. Wood, Living Rev. Solar Phys. **1**, 2 (2004).

[82] N. Gopalswamy, A. Lara, S. Yashiro, M. L. Kaiser, and R. A. Howard, J. Geophys. Res. **106**, 29207 (2001).

[83] P. K. Manoharan, Sol. Phys. **235**, 345 (2006).

[84] K.-H. Kim, Y.-J. Moon, and K.-S. Cho, J. Geophys. Res. **112**, 5104 (2007).

[85] B. Vršnak and T. Žic, Astron. Astrophys. **472**, 937 (2007).

[86] B. Vršnak, T. Žic, T. V. Falkenberg, C. Möstl, S. Vennerstrom, and D. Vrbanec, Astron. Astrophys. **512**, A43 (2010).

[87] M. Temmer, T. Rollett, C. Möstl, A. M. Veronig, B. Vršnak, and D. Odstrčil, Astrophys. J. **743**, 101 (2011).

[88] S. Jang, Y.-J. Moon, J.-O. Lee, and H. Na, J. Geophys. Res. **119**, 7120 (2014).

[89] X. Zhao and M. Dryer, Space Weather **12**, 448 (2014).

[90] J. Liu, Y. Ye, C. Shen, Y. Wang, and R. Erdélyi, Astrophys. J. **855**, 109 (2018).

[91] P. A. Sturrock and R. E. Hartle, Phys. Rev. Lett. **16**, 628 (1966).

[92] B. Li, L. D. Xia, and Y. Chen, Astron. Astrophys. **529**, A148 (2011).

[93] S. R. Cranmer, Space Sci. Rev. **172**, 145 (2012).

[94] A. V. Usmanov, M. L. Goldstein, and W. H. Matthaeus, Astrophys. J. **788**, 43 (2014).

[95] R. F. Pinto and A. P. Rouillard, Astrophys. J. **838**, 89 (2017).